Quantifying Impedance in Conceptual Models of Pleistocene Glacial Cycles

Lillian Stensland

Department of Mathematics

California Polytechnic State University

San Luis Obispo, California

June 2024

APPROVAL PAGE

TITLE: Quantifying Impedance in Conceptual Models of Pleistocene Glacial Cycles

AUTHORS: Lillian Stensland

DATE SUBMITTED: June 2024

Charles D. Camp

Senior Project Advisor

Signature

Ben Richert

Mathematics Department Chair

Signature

Abstract

The Mid Pleistocene Transition (MPT), during which the timescales of glacial cycles shifted from ∼40 kyr to ∼100 kyr, is a widely researched yet continually unsolved issue for scientists of Earth's paleoclimate. Obliquity, an orbital parameter which contributes to the pacing of glacial cycles, triggered a full system melt with every cycle during the early Pleistocene. However, as the MPT progressed, the trigger of full system melts began to skip obliquity cycles, contributing to the longer timescale of the late Pleistocene. A hypothesized cause of this behavior is the impedance phenomenon, where there was an increase in the climate system's internal resiliency to changes in obliquity.

This paper seeks to quantify impedance in the PP04 conceptual climate model, as presented in Paillard & Parrenin (2004). Three geometric measures are given, which explore the internal impedance of the model and can represent the impedance evident in model runs perturbed by any random forcing term. Two measures are given which look at the response of the PP04 model to realistic forcing. Currently, impedance is only loosely defined, opening avenues for future study in further developing the definition or quantification measures of impedance. Impedance measures could, with further development, be useful as a tool for model validation.

Acknowledgements

This research was generously supported by the William and Linda Frost Fund in the Cal Poly Bailey College of Science and Mathematics. Additionally, fellow Cal Poly student Connor Fletcher contributed to much of the development of the dot-product impedance measure.

Contents

1 Introduction

Around 2.6 million years ago, marking the beginning of the Pleistocene, Earth's climate began to experience semi-regular cycles of cool and warm global temperatures, creating glacial growth (glaciation) and glacial decay (deglaciation). These glacial growth-decay cycles are characterized by continental ice sheets and polar ice caps melting into ice-free poles, then replenishing the ice on a semi-regular timescale (Zachos et. al., 2001; PAGES, 2016; Berends et. al., 2021; Lisiecki & Raymo, 2005). Multiple processes on Earth interact to produce such cycles, including tectonic plate movement and chemical evolutions within both the ocean and the atmosphere; each deglaciation is marked by specific changes in these processes, such as falls in marine oxygen isotope ratios, atmospheric carbon dioxide and methane concentration increases, and increased air temperatures (Von der Heydt et. al., 2021; Zachos et. al., 2001; PAGES, 2016).

Researchers have divided the Pleistocene into two intervals, early and late. Lisiecki & Raymo (2005) built a data record of the Pleistocene using oxygen isotopes, called δ^{18}O , which can be used as a proxy for global ice volume. High measures of δ^{18}O are associated with lower temperatures, and thus glaciation, while low measures of δ^{18}O are associated with high temperatures, and thus deglaciation. Figure 1 shows the δ^{18}O record, exhibiting the $\sim$40 kyr timescale of glacial cycles which occur during the early Pleistocene, as well as the much stronger cycles with a $\sim$100 kyr timescale that characterize the late Pleistocene. The transition from the early to late Pleistocene, known as the Mid Pleistocene Transition (MPT), was gradual, beginning about 1.2 million years ago and ending about 0.6 million years later, marked in gray on Figure 1 (Berends et. al., 2021; PAGES, 2016). Besides an increased timescale, glacial cycles after the MPT are also characterized by a strong asymmetry. Deglaciations occur much more rapidly than glaciations, reflected in the data as a 'sawtooth' pattern (PAGES, 2016; De Saedeleer et. al., 2012). On average, glacial growth lasts around 90 kyr, while glacial decay lasts only around 10 kyr (Raymo & Huybers, 2008). While the cause of the MPT remains unknown, several theories have been proposed, such as a manifestation of a bifurcation within the system, a global cooling trend allowing for ice-sheets to reach a size threshold to resist melting, or even a spontaneous period-doubling effect (Berends et.

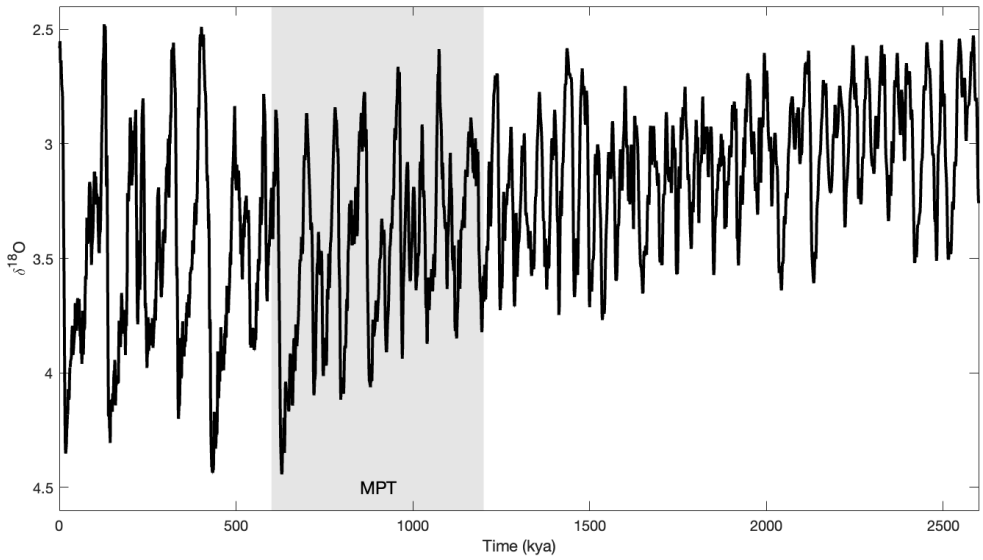

Figure 1: The LR04 stack, averaging measures from 57 sites of deep sea δ^{18}O , as a proxy for global ice volume. The Mid Pleistocene Transition, highlighted in gray, falls between the late Pleistocene (left) and the early Pleistocene (right). Note that the vertical axis reverses the δ^{18}O scale, to show correlated warm global temperatures at the top and cool global temperatures at the bottom.

al., 2021; Von der Heydt et. al., 2021).

When discussing the MPT, researchers often consider Earth's interactions with external solar radiation, called insolation, which combines the variations in the following orbital parameters: eccentricity, obliquity, and precession (with dominant timescales of ∼100 kyr, ∼40 kyr, and ∼20 kyr respectively) (Von der Heydt et. al., 2021; Ashkenazy & Gildor, 2008). Two main theories exist for the importance of insolation to Earth's climate system (Ashkenazy & Gildor, 2008; Milankovitch, 1998; Hays et. al., 1976; Crucifix et. al., 2020):

1. Strong Milankovitch theory, where glacial cycles are created by insolation, or

2. Weak Milankovitch theory, where cycles occur due to the dynamics of the internal climate system and insolation acts to time, or pace, the oscillations.

The variations in eccentricity within insolation are weak, implying that strong Milankovitch theory cannot explain the ∼100 kyr cycles evident in the late Pleistocene, as the climate record sees the power of the ∼100 kyr frequency increase during the MPT while the power of eccentricity remains

small within insolation (Gildor & Tziperman, 2000; Lisiecki, 2010). However, weak Milankovich theory seems to provide a plausible explanation for the behavior of glacial cycles, both before and after the MPT. In Huybers (2007), the climate record analysis related to this theory explores the increasing tendency for deglaciations to skip large insolation events, coordinating to skipped obliquity cycles, as the climate system's interactions with insolation changes. Some unspecified changing facet of the system creates growing impedance to the triggering of a full glacial melt by the obliquity cycles within insolation.

Conceptual climate models are a common tool used to investigate the behavior and interactions of Earth's climate system. Such models typically incorporate the interactions between internal glacial cycles and external solar forcing through low-order dynamical systems. Some models, for example, rely on bifurcation theory to show the transition from the Early to the Late Pleistocene, as a bifurcation can create a limit cycle (Saltzman & Maasch, 1990, 1991). Other models rely on relaxation dynamics to constantly evolving limit cycles that represent the fast and slow timescales evident in the asymmetry of glacial cycles (Paillard, 1998; Gildor & Tziperman, 2000; Paillard & Parrenin, 2004).

In this paper, the theory of skipped obliquity cycles is investigated within Earth's glacial cycles, utilizing a conceptual climate model. The purpose of this work is to find useful ways to quantify impedance within a conceptual climate model, to eventually be able to use these measures as a method of model validation. Section 2 explores data and modeling tools. Section 3 follows by defining and illustrating the impedance phenomenon qualitatively. Section 4 introduces various methods of quantifying impedance within a model, either as a response to general forcing or as a response to targeted, more realistic forcing. Finally, Section 5 discusses various findings and conclusions, and introduces lines of future work and remaining open questions.

2 Data & Modeling

2.1 Data Record

In order to study these paleoclimate processes, researchers rely on deep sea oxygen isotope ratios as proxy data sets for changing ice volume. The ratio between standard oxygen-16 and oxygen-18 isotope (denoted δ^{18}O), as recorded from deep ocean sediments, is related to global temperature and water salinity, and these measurements have an observed similarity to global ice volume, allowing for researchers to determine common timescales of glacial phenomena (Lisiecki & Raymo, 2005; Imbrie et. al., 1984). δ^{18}O acts as a proxy for global ice volume, with high amounts correlating to cooling within the climate system, and low amounts of δ^{18}O correlating to warming. A measure with high resolution of deep sea δ^{18}O over the Pleistocene is recorded in the LR04 stack, presented by Lisiecki & Raymo (2005), which averages measures from 57 well-distributed sites in the Atlantic, Pacific, and Indian Oceans. This stack, as presented in Figure 1, spans 5.3 million years, and is useful when attempting to measure dominant periodicity and relative timescales of Earth's climate system.

During the early Pleistocene, glacial cycles were triggered by the maximum of nearly every obliquity cycle; only occasionally did a high obliquity event fail to trigger an deglaciation (Huybers, 2007). As the climate system transitioned into the late Pleistocene, the frequency of high obliquity trigger-failure increased, resulting in deglaciations skipping 1-2 obliquity cycles on a regular basis. Thus, glacial cycles paced by the ∼40 kyr obliquity signal saw an increase in timescale that averages ∼100 kyr. Data signals which combine differing powers of multiple periodic functions can be analyzed using an ensemble empirical mode decomposition (EEMD), as in Von der Heydt et. al. (2021). The data is decomposed into intrinsic mode functions (IMFs) which exhibit the relative power of each frequency within the data. Through an EEMD analysis of the LR04 data record, presented in Figure 2, the MPT becomes evident, as the dominant frequency of ∼40 kyr lasts up until the instigation of the MPT at ∼1.2 Myr ago and then changes to be ∼100 kyr. Notably, the ∼40 kyr timescale does not vanish in the late Pleistocene when it is no longer dominant, but instead becomes irregular and weaker (Von der Heydt et. al., 2021). The ∼40 kyr timescale is thus said

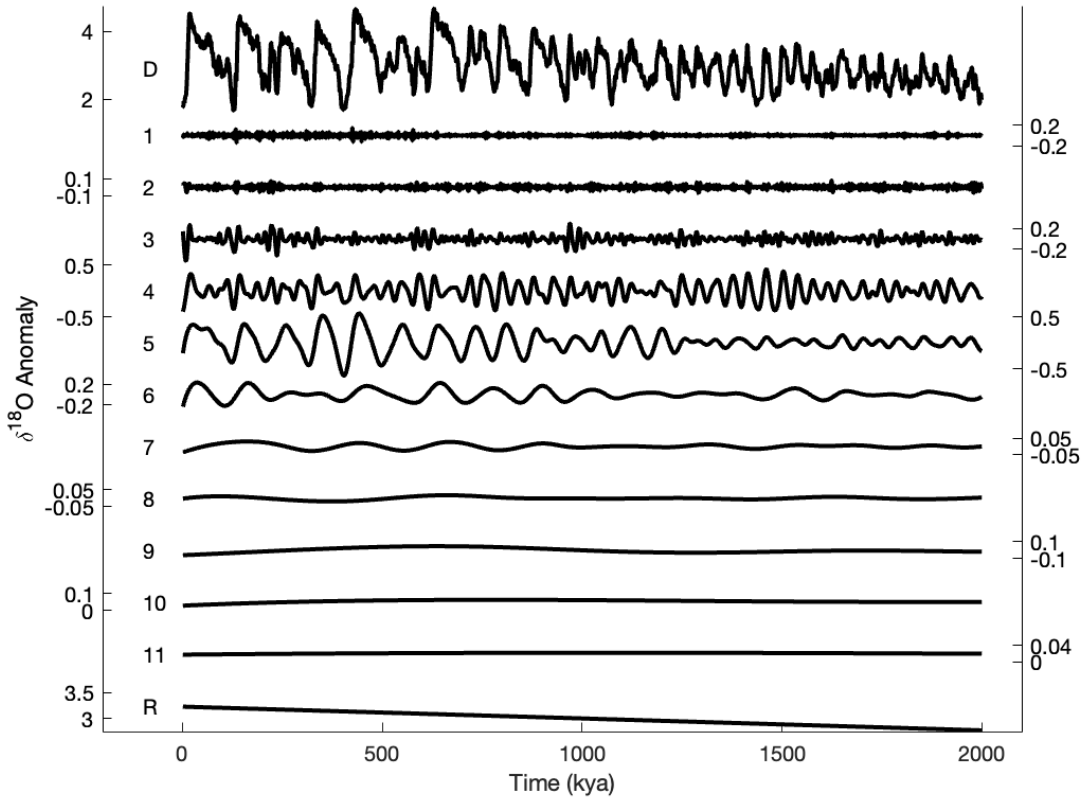

Figure 2: An EEMD analysis of the LR04 stack, ran with 0.5 noise and 2500 iterations. The 'D' curve is the original data with a small amount of added noise, while the following IMFs decompose the LR04 stack, from shortest to longest timescale. IMF 4 has a timescale similar to obliquity (∼40 kyr), while IMF 5 exhibits a timescale similar to the late Pleistocene (*sim*100 kyr).

to be persistent, while the ∼100 kyr timescale is said to be emergent. Without a clear relationship between the amplitude of an obliquity cycle and the strength of a glacial melt, Huybers (2007) proposed that the internal climate system itself changed, resulting in skipped obliquity cycles.

Through data analysis of a δ^{18}O stack, Huybers (2007) conluded that a sudden bifurcation or other swift transition leading to the switch from a ∼40 kyr timescale to a ∼100 kyr timescale was unsupported by the behavior of the climate system. Instead, a slow evolution of the system created cooling that impedes the ability of high insolation to trigger a deglaciation. To show this internal change, Huybers (2007) created a simple conceptual model, where ice volume increases until it reaches a threshold and is then reset to 0. The threshold depends on the obliquity curve with an

introduced linear drift component. The model equations are presented:

$$\begin{aligned} V_t &= V_{t-1} + \eta_t \text{ and if } V_t \geq T_t \text{ terminate,} \\ T_t &= at + b - c\theta'_t \end{aligned} \tag{1}$$

This model exhibits oscillatory behavior which mimics, in a rudimentary fashion, glacial cycles, with steady ice growth and rapid melts. Ice volume, represented by the V_t equation, grows by a random variable η_t, which has a mean of 1 and standard deviation of 0.5. The T_t equation refers to the ice threshold, and when the V_t curve touches the T_t curve, the glaciation is terminated, and thus V_t resets to zero over the immediate 10,000 years. As evident in Figure 3, glacial termination occurs with every obliquity cycle up to ∼0.8 Myr ago, as the ice volume line (black) makes contact with the blue threshold curve. After ∼0.8 Myr ago, which occurs during the MPT, glacial cycles begin to skip 1-2 obliquity cycles. The downward drift of the threshold curve represents the climate system's trend towards longer glacial cycles despite relatively unchanged orbital dynamics. However, an open question remains as to what causes this trend towards skipped obliquity and the related impedance of deglaciations.

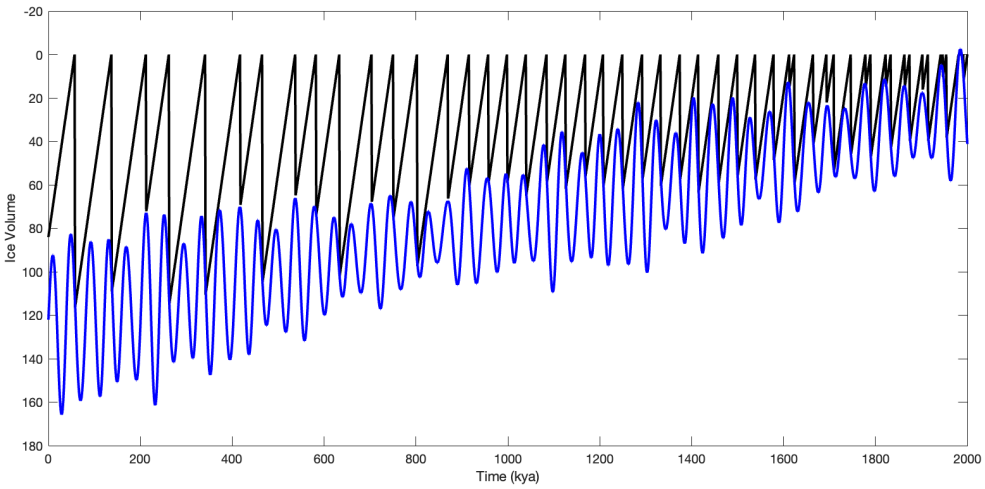

Figure 3: The simple oscillatory threshold model presented in Huybers (2007). The threshold curve (blue) triggers a melt in the system when it contacts the ice volume curve (black).

The climate system became characterized by deep ice ages, with a sawtooth data pattern rep-

resenting long glacial growth and sharp glacial decay (PAGES, 2016). During the Late Pleistocene, the climate system experiences what can be called a 'full melt' with ∼100 kyr timescale, where most or all of the ice present in the system melts. Between successive full melts, during an interval of glacial growth, the system often exhibits partial melts, where some of the ice melts away before continuing to rebuild. Further EEMD analysis of the LR04 stack can exhibit this phenomenon. Figure 4 combines the most prominent frequencies within the LR04 data set, to show each large, full-system melt occurring every ∼100 kyr, with ice growth characterized by small melts followed by continued ice growth. For example, at 127 kya, δ^{18}O decreases to -0.94, then begins to rebuild, only to experience three smaller melts before the δ^{18}O is reaches a maximum of 0.95 at 19 kya.

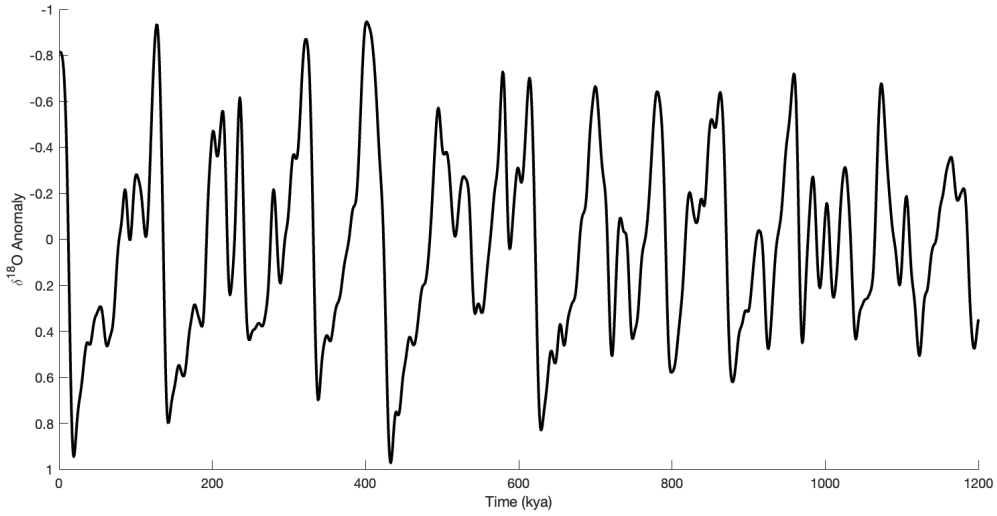

Figure 4: An EEMD bandpass-filter of the LR04 stack, combining the 3rd through 7th IMFs. A low δ^{18}O anomaly is correlated with higher temperatures, while a high δ^{18}O anomaly is correlated with lower temperatures.

2.2 Modeling

2.2.1 Conceptual Climate Models

Due to limited paleoclimate records and an inability to recreate Earth's glacial cycles in a laboratory setting, researchers turn to climate models to represent the spatial and temporal scales as well as the physical processes which take place in the climate system (Von der Heydt et. al., 2021). Models

are classified depending on the number of scales and processes they contain. The simplest group are called conceptual climate models, which describe only specific interactions within the climate system. By discretizing the differential equations within a model, additional scales can be added to create an intermediate complexity model. Finally, Global Climate models increase the number of processes to create a high resolution representation of Earth's climate system.

While various types of models offer useful insights into the climate system, conceptual climate models are particularly helpful in understanding critical aspects of glacial cycles (Leloup & Paillard, 2022; Von der Heydt et. al., 2021). The behavior of complex systems in one scale can be captured with systems of differential equations, often limited to two or three dimensions, which contain a globally attracting limit cycle that can be interpreted as Earth's glacial cycles (Crucifix, 2012). By studying the response of the system to astronomical (insolation) forcing, researchers are able to draw conclusions and create hypotheses about the climate system.

Conceptual climate models often seek to model glacial cycles of both the early and late Pleistocene by introducing tunable parameters, which change the timescale and behavior of cycles depending on the values. Additionally, some models, referred to as 'non-smooth models,' experience a discontinuity when running the model equations. For example, some non-smooth models display cool glaciation intervals separate from warm intervals of deglaciation by including a model switch depending on whether the output should represent warming or cooling. In contrast, 'smooth' models experience no discontinuities, and can use one set of equations to model both glaciations and deglaciations. In more complex models, researchers can consider the effects of unresolved processes on model variables by introducing a parameter drift, for slow processes, and stochastic terms, for fast processes (Crucifix, 2012).

2.2.2 Synchronization

Dynamical systems present unique challenges to modeling Earth's climate system. When introducing a forcing term with varied powers of frequencies to a system of differential equations, such as insolation forcing in a conceptual climate model, multiple initial conditions will converge to attracting trajectories, as seen in Figure 5 (De Saedeleer et. al., 2012; Tziperman et. al., 2006).

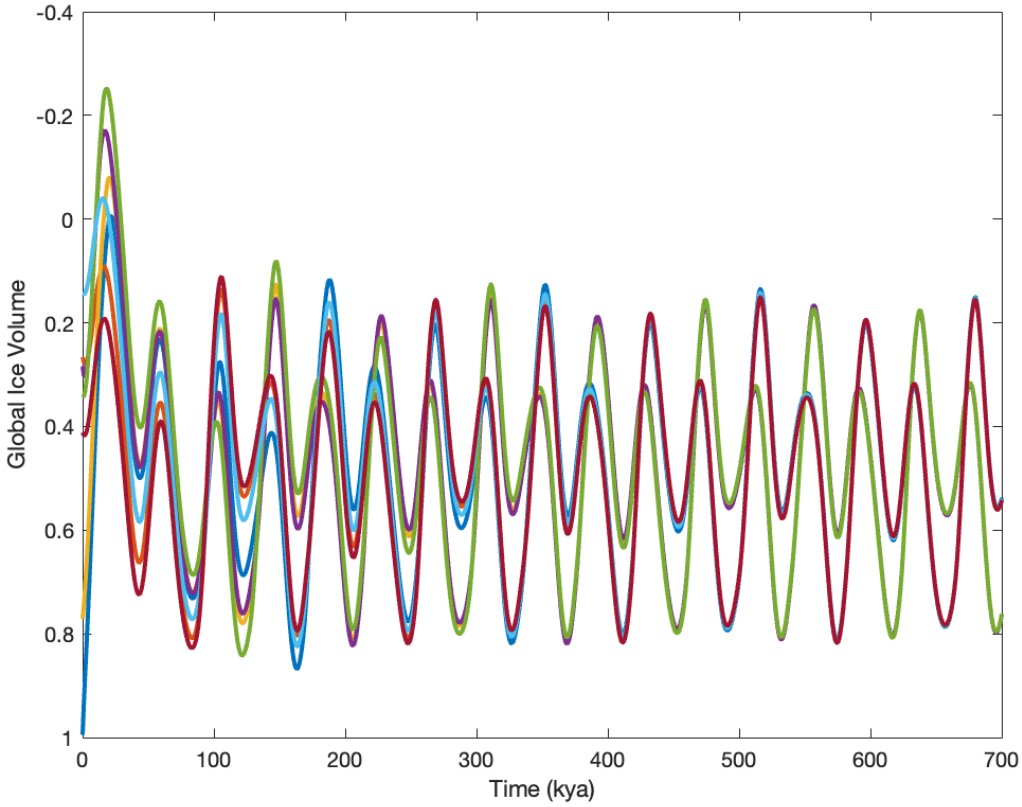

Figure 5: Synchronization on the PP04 model. Seven trajectories of the PP04 model with different initial conditions that converge to two trajectories.

This phenomenon, called non-linear phase locking or synchronization, exhibits a quantized period for output trajectories, where the output period of the synchronized trajectories is some rational multiple of the dominant timescale of the forcing term. As a result of synchronization, unrealistic climate models, which are not meant to accurately show glacial cycle behavior, can be phase-locked to fit the timescales of data records and thus produce realistic results.

2.3 A Non-Smooth Sea Ice Model

This paper relies on the model developed in the Paillard & Parrenin (2004) paper, referred to as the PP04 model. As a 3-dimensional climate model, PP04 looks at interactions between ice volume, carbon dioxide, and deep-water brine levels. The three variables are global ice volume (V), area

of the Antarctic ice sheet (A), and atmospheric CO_2 (C). These variables reflect the cyclic change in global ice, in which a maximum in V is followed by a delayed maximum in A. At this point, salt within the ocean is less likely to sink and contribute to deep-water brine, which slows ocean circulation and decreases absorption of gases like CO_2 by the ocean. This, in turn, increases C and global temperatures, thus ultimately decreasing V followed by A. The deep-water brine is represented as a model switch, which turns on a heaviside function when deep-water brine sits at deglaciation levels. The relaxation equations representing this behavior are presented here:

$$\begin{aligned} dV/dt &= (V_R - V)/\tau_V \\ dA/dt &= (V - A)/\tau_A \\ dC/dt &= (C_R - C)/\tau_C \end{aligned} \tag{2}$$

Where,

$$\begin{aligned} V_R &= -xC - yI_{65} + z \\ C_R &= \alpha I_{65} - \beta V + \gamma H(-F) + \delta \\ F &= aV - bA - cI_{60} + d \\ H &= \begin{cases} 1 & \text{if } F < 0 \\ 0 & \text{otherwise} \end{cases} \end{aligned} \tag{3}$$

Table 1: Default Parameters of the PP04 Model

Parameter	Value	Parameter	Value
τ_V	15 (kyr)	x	1.3
τ_C	5 (kyr)	y	0.5
τ_A	12 (kyr)	z	0.8
α	0.15	a	0.3
β	0.5	b	0.7
γ	0.5	c	0.0
δ	0.4	d	0.27

The F equation creates warming or cooling in the PP04 model by changing the target CO_2 levels, thus changing global temperatures. If c=0, F creates a plane in 3D space. When projected

onto the V vs A plane, as seen in Figure 6, the F equation creates a line (hereafter referred to as the trigger line) which draws a clear split between the warming (red) and cooling (blue) states of the PP04 limit cycle. By changing the drift parameter, d, the model can represent different eras of the Pleistocene. With the default value of $d = 0.27$, the PP04 model, without any applied astronomical forcing, creates 132 kyr limit cycles, which can represent the glacial cycles of the late Pleistocene. These limit cycles are asymmetric, with only ∼20 kyr spent in the warming state.

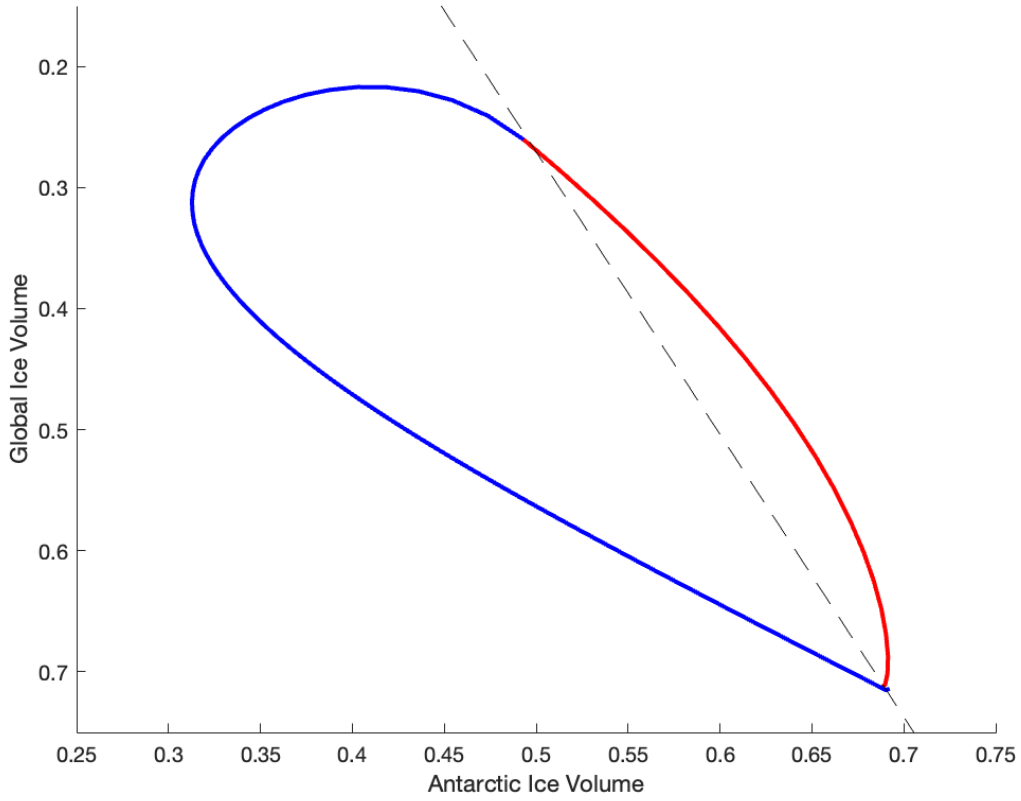

Figure 6: Limit cycle for the unforced PP04 model, with default parameters, projected on the Global Ice Volume (V) vs Antarctic Ice Volume (A) plane. The trigger line created by the F equation (black, dotted), splits the limit cycle between the warming (red) and cooling (blue) model states. The total period of the limit cycle is 132 kyr, with 20 kyr spent in the warming state and 112 kyr spent in the cooling state

3 Defining Impedance Qualitatively

Skipped obliquity cycles manifest in the climate system as partial melts between successive full melts, as discussed above. In the early Pleistocene, each obliquity cycle triggered a full system melt; however as time passed something changed in the system, leading to skipped obliquity cycles. A hypothesis arises from this behavior: the climate system's internal resiliency to high insolation events (specifically related to obliquity cycles) increased during the MPT. This phenomenon, referred to as impedance, is a promising theory for the transition to the deeper, longer ice ages which characterize the climate system after the MPT.

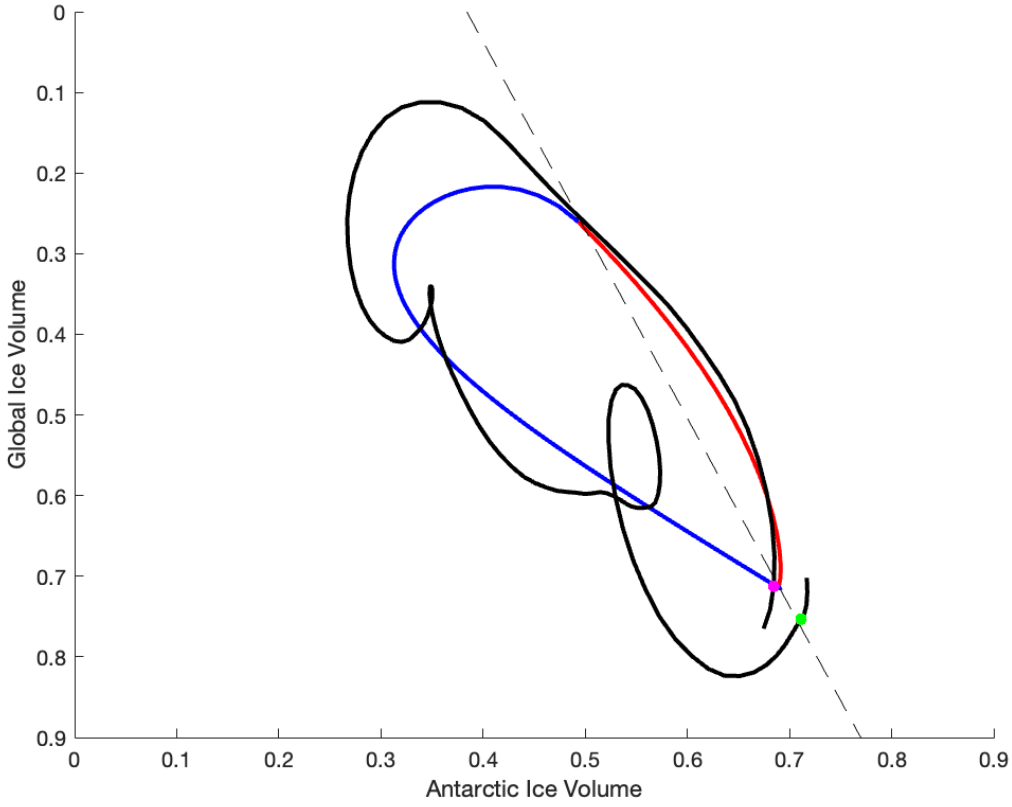

Figure 7: A forced PP04 cycle, using integrated insolation, overlaid on the PP04 limit cycle. The glacial cycle begins at the pink dot and ends at the green dot. The model was run using default parameters, with the exception of $y = 0.25$ and $\alpha = 0.075$.

Due to synchronization, conceptual climate models can be tuned to produce realistic results,

regardless of how unrealistic the model is. Thus, methods other than simple comparison of model output to data are required to validate models. Because impedance seems to be a clear feature of the climate system, a reliable occurrence of impedance in a model could help to validate a conceptual model.

In order to develop this model validation tool, impedance within a model must first be identified. Within the forced PP04 model, partial melts occur between full melts in the time series output. Additionally, on the V vs A projection, partial melts can been seen as loops during the cooling state of the model, such as in Figure 7. Here, the glacial cycle begins with the global ice melting and then beginning to regrow, only to melt off slightly and regrow twice before the cycle ends. Figure 8a shows the entire cycle in a time series, beginning ∼1950 kya and ending ∼1830 kya. Both of the partial melts align with the skipped insolation events at ∼1900 and ∼1860 kya, shown in Figure 8b. In the following sections, this paper will explore different methods of quantifying the impedance within the PP04 model.

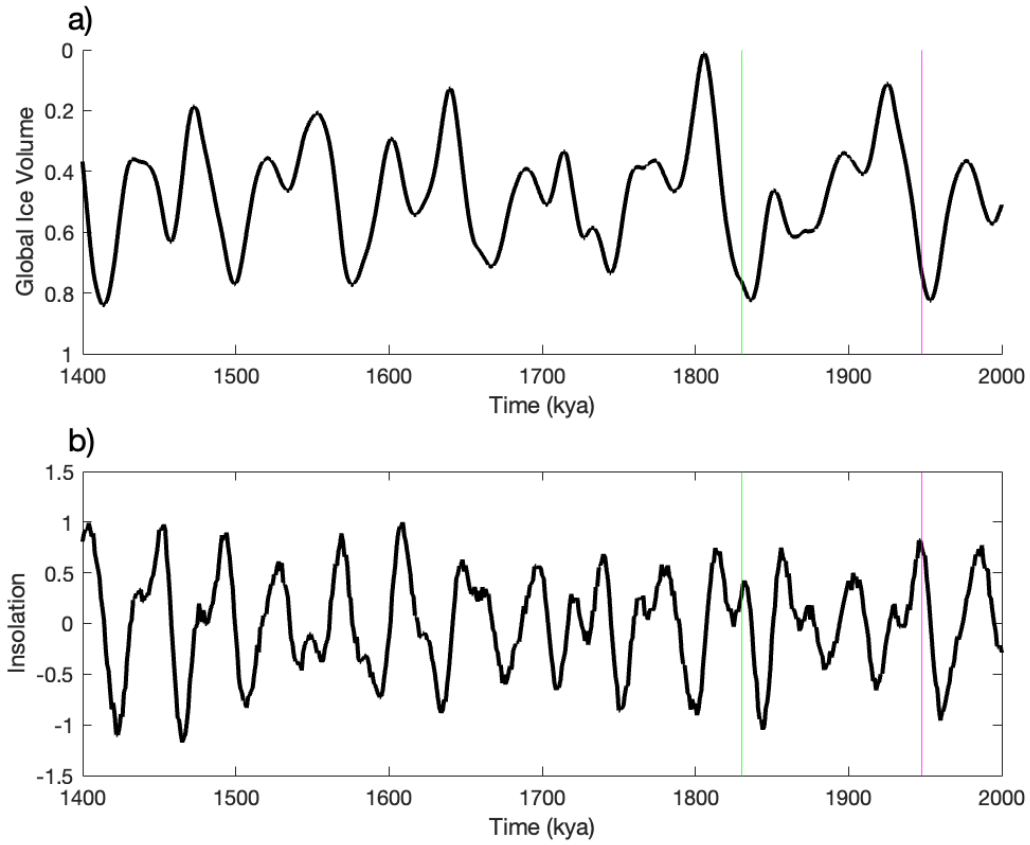

Figure 8: **(a)** A time series representation of the PP04 model forced with integrated insolation. The cycle beginning at the pink line and ending at the green line is overlaid on the PP04 limit cycle in Figure 7. **(b)** The integrated insolation curve used to force the PP04 model.

4 Defining Impedance Quantitatively

4.1 Geometric

Conceptual climate models have an internal oscillatory structure which can be forced with realistic insolation forcing to mimic the behavior of the glacial system. The climate system's response to an arbitrary forcing term, and thus the impedance inherent to the system, can be explored by analyzing the unforced model. To do this, three geometric methods of measuring impedance are introduced: distance to the trigger line, point perturbation, and gradient perturbation.

4.1.1 Distance to the Trigger Line

One simple measure of impedance within a model relies on the distance to the trigger line. By taking each point on the unforced limit cycle of the PP04 model and calculating the distance to the trigger line, the internal geometry of the system can be considered as a source of impedance. With this measure, the minimum distance required for a trajectory to switch from the model's cooling state to its warming state is the impedance of the system, as shown in Figure 9a.

Figure 9b shows the change in impedance throughout the PP04 limit cycle. This measure shows the largest amount of impedance near the middle of the cooling section of the model, in the same location where partial melts tend to occur in a model run. This is to be expected, as impedance to the system prevents the obliquity cycle from triggering a full melt. This impedance measure simply looks at the internal climate system, and does not consider the immediate effect of adding forcing to the system. In order to explore this interaction, a new impedance measure is introduced.

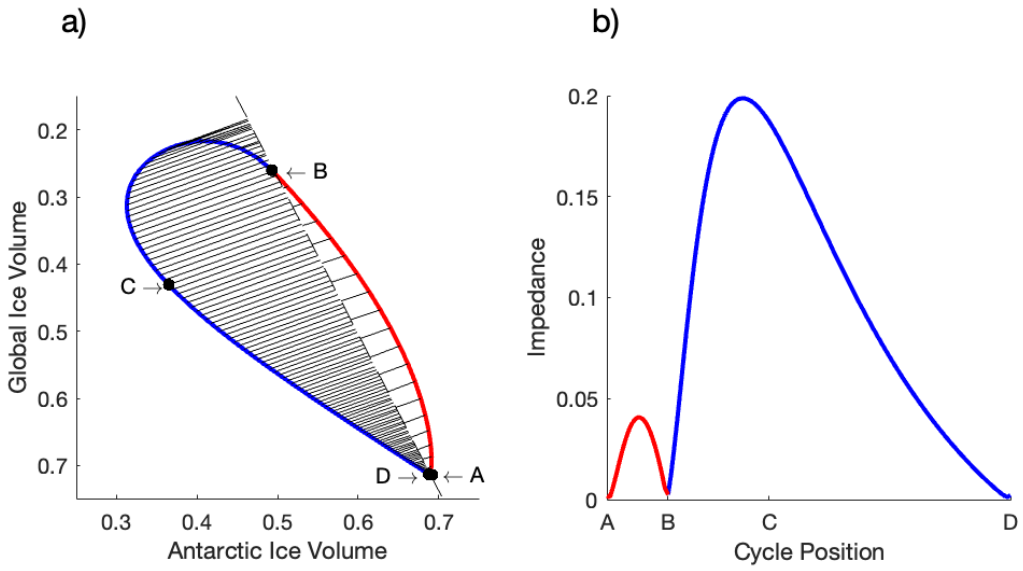

Figure 9: A geometric measure of impedance as distance to the trigger line. **(a)** For each point on the limit cycle, a (black) line denotes the shortest distance to the trigger line. **(b)** The shortest distance from each point on the limit cycle, beginning at point A and traveling counter-clockwise to end at point D.

4.1.2 Point Perturbation

Rather than calculating the distance to the trigger line, each point on the PP04 limit cycle is perturbed with a random sample of 10,000 vectors, to explore the instantaneous effect of forcing on the climate system, as shown in Figure 10a. Under this measure, impedance is the proportion of perturbed points which do not cross the trigger line, or the proportion of trajectories which would not result in the model switching to the warming state and thus creating a full melt.

This measure, as evident in Figure 10b, creates similar results as the previous. However, impedance is greater for a larger portion of the cooling section of the PP04 model, seeming to show that partial melts are even more likely to occur than suggested by the distance measure. While this impedance measure looks at the immediate effect of a random forcing vector, it does not take into account the bias in direction of travel that system trajectories (forced or unforced) will have.

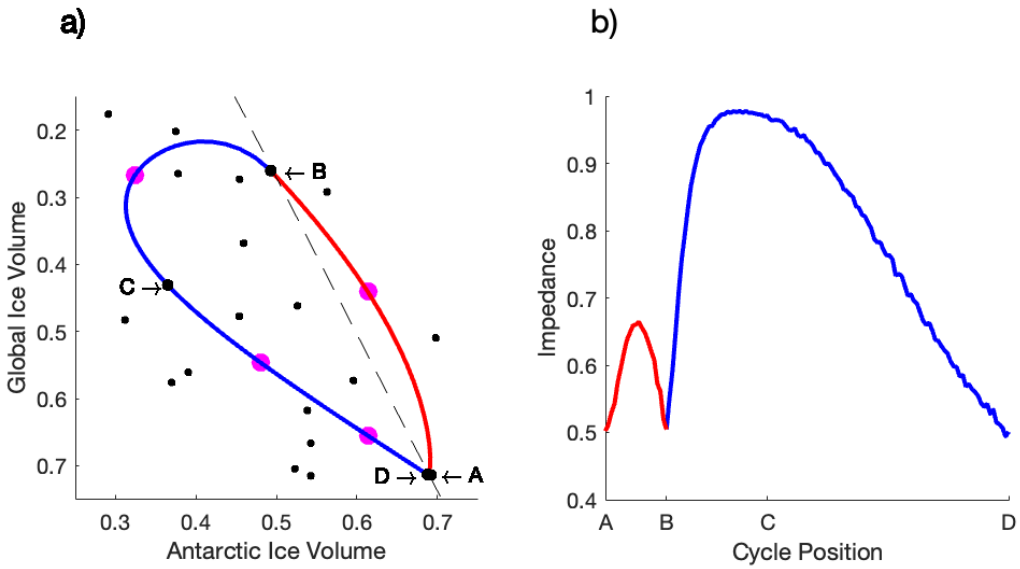

Figure 10: A measure of impedance utilizing point perturbation. **(a)** A selection of four points on the limit cycle (denoted with pink dots) with five representative point perturbations each (denoted with black dots). **(b)** The proportion of perturbed points which do not cross the trigger line for each point on the limit cycle, beginning at point A and traveling counter-clockwise to end at point D.

4.1.3 Gradient Perturbation

In order to account for the model's natural direction of travel, as well as the instantaneous effect of forcing, the unforced gradient vectors at each point on the limit cycle are perturbed with a sample of 10,000 random vectors, as shown in Figure 11a. Then, similar to the point perturbation method, impedance is the proportion of perturbed gradient vectors which do not cross the trigger line.

Figure 11b shows similar results as both of the previous measures, but with an even larger portion of the cooling section of the model exhibiting high impedance. All three of the geometric measures of impedance do not account for the nonlinear effects of forcing over time, thus requiring the development of a new measure which looks at the impedance resulting from various, targeted choices of forcing terms.

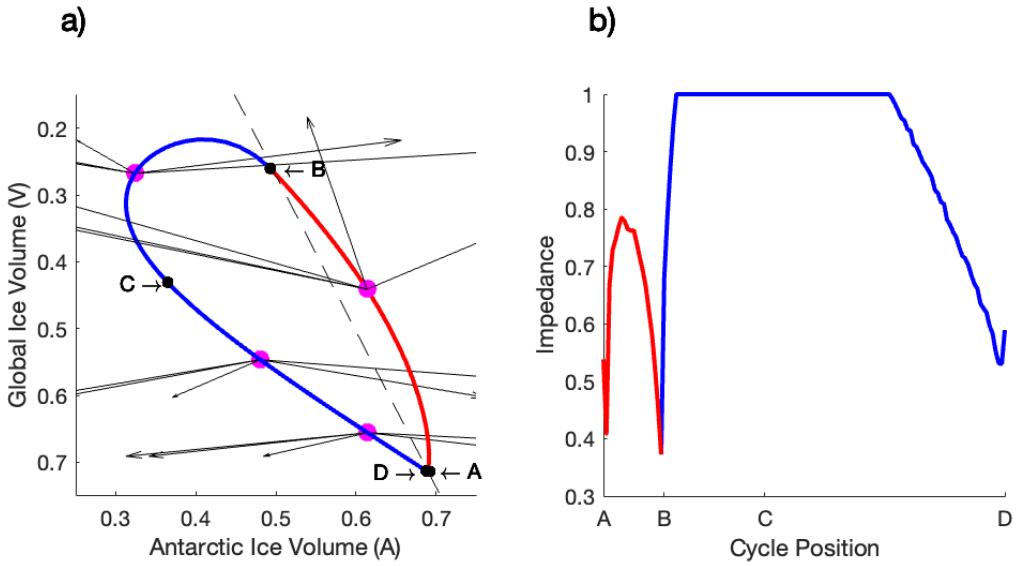

Figure 11: A measure of impedance utilizing gradient perturbation. **(a)** A selection of four points on the limit cycle (denoted with pink dots) with five representative gradient perturbations each (denoted with black arrows). **(b)** The proportion of perturbed gradients which do not cross the trigger line for each point on the limit cycle, beginning at point A and traveling counter-clockwise to end at point D.

4.2 Targeted Impedance

In order to explore a more targeted version of impedance, the PP04 model's response to realistic forcing is explored. To achieve this, two tasks are required: first, creating a population of high insolation events to draw samples from; second, creating a measure of the impedance in the model's response to the samples.

4.2.1 Defining High Insolation Events

In order to create a population from which to pull high insolation forcing samples, a decision must first be made on how to build an appropriate insolation curve for a conceptual model. Models of past and future insolation are based upon models of the Earth's orbital parameters. Laskar et. al. (2004) provides accurate values for insolation spanning from 250 Myr ago to 250 Myr in the future. However, the Laskar model does not provide the daily insolation model needed for some calculations of insolation forcing signals. Meanwhile, Berger (1978) provides a framework for creating an analytic approximation of the orbital parameters which make up insolation, with only minor differences in value over the span of 1 Myr ago to 100 kyr in the future. This timespan ensures that the parameter values can represent the system at the point of growing impedance, during the MPT and late Pleistocene. Each orbital parameter can be approximated with a trigonometric-series expansion of varying lengths (obliquity consists of 47 terms, eccentricity consists of 19 terms, and precession consists of 78 terms). The results of these expansions can be converted into daily insolation efficiently.

Traditional insolation curves are averaged to represent the changing insolation, with measurements taken at 65° N corresponding to the rim of northern ice sheets (Von der Heydt et. al., 2021). However, averaging insolation is an imprecise process. Temperatures outside of northern summer are largely irrelevant, so only mean summer insolation needs to be calculated. But, the length of summer changes depending on insolation itself, with large insolation cycles leading to short summers (Huybers, 2006; Raymo & Huybers, 2008). A common proxy is to represent the changes in mean summer insolation by the changes in summer solstice insolation, but this overemphasizes the precessional component compared to the obliquity component. To combat this challenge, Huybers

(2006) introduced the integrated insolation method. By setting a threshold intensity at 275 W/m^2, any day in one year with insolation falling above this threshold can be included in the sum, creating an annual insolation value. Taking each annual value over some period of time creates an insolation curve with a dominant obliquity component. In this paper, the insolation curve was created using 1kyr timesteps. The resulting insolation curve is presented in Figure 12a. In order to ensure proper power of the forcing within the PP04 model, the y and α parameters were changed to 0.25 and 0.075 in model runs.

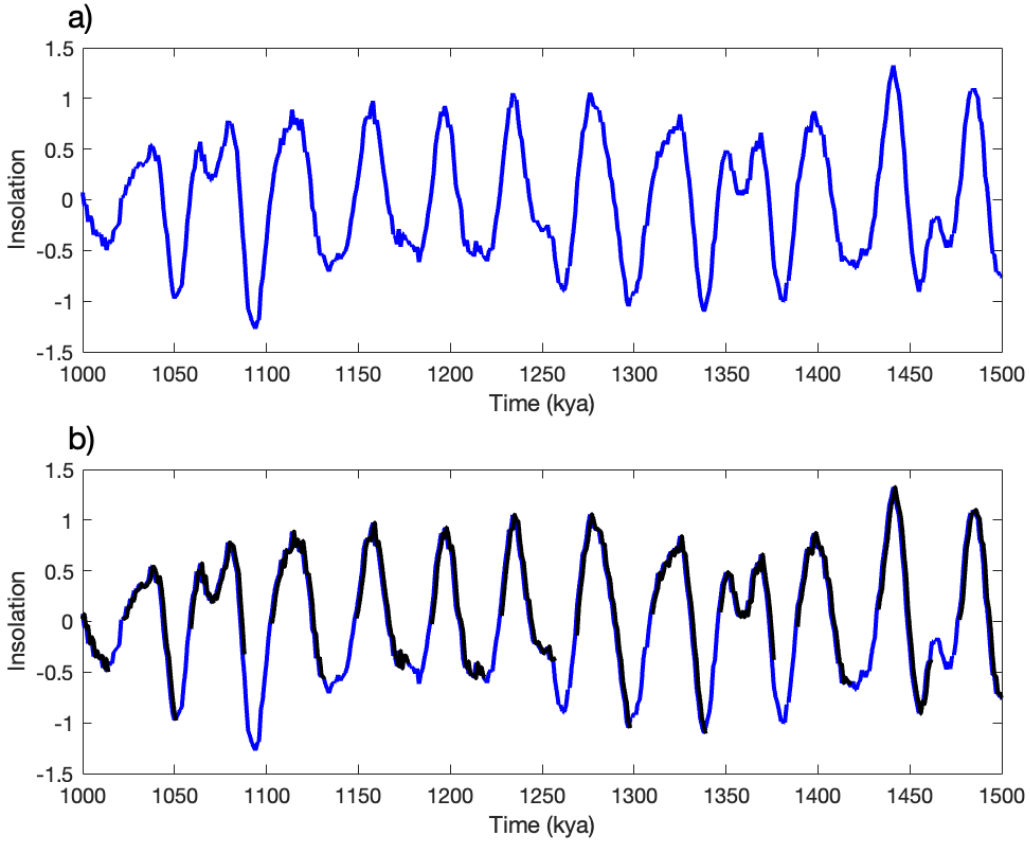

Figure 12: **(a)** The integrated insolation forcing curve. **(b)** 13 forcing samples (black) overlayed on the integrated insolation forcing curve (blue).

By nature of this creation method, the insolation curve can be extended for any length of time. However, when compared to astronomical values, the orbital parameters exhibit differences of up to 4.5% for the last one million years, with the differences increasing beyond this time frame (Berger,

1978). Thus, the extended insolation curve creates insolation forcing representative of the post-MPT time period studied, but does not create realistic forcing beyond 1 million years ago. The extended insolation curve is useful for pulling forcing samples, but any samples pulled inside the accuracy window should be considered realistic.

From the insolation curve, a population from which to pull forcing samples can be created. In this paper, each high insolation event is defined by the following procedure:

1. Find each zero crossing at which the insolation curve is increasing.

2. Collect insolation data for the next 30 kyrs, capturing a local maxima.

In a 400 Myr insolation record, this process of defining high insolation events creates a population of 12,350 events. The samples pulled between ∼1500 and ∼1000 kya are presented in black, overlaid on the original insolation curve (blue), in Figure 12b. Presented in Figure 13, analysis of the high insolation event population shows a relatively normal spread for the maximum value of each event, a value which tends to occur in the first 15,000 years of an event.

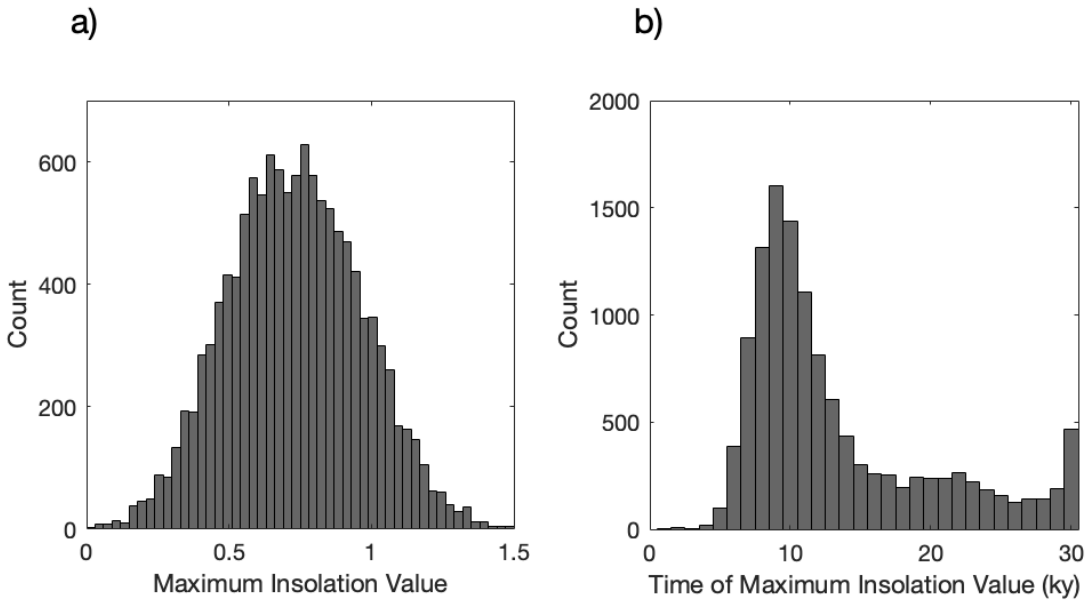

Figure 13: Analysis of the population of high insolation events. **(a)** A histogram of the maximum value within each high insolation event. **(b)** A histogram of the time within an event at which each maximum value occurs.

4.2.2 Net Ice Loss

Introducing a length 30 kyr forcing sample to the PP04 model creates an output also of length 30 kyr, shown in Figure 14a. If the model experiences a full melt in response to a forcing sample, all or most of the ice will be lost throughout the model run. However, if the model experiences a partial melt, time must be dedicated to rebuilding the lost ice rather than melting. Thus, model output can be sorted depending on melt size based on ice loss. By measuring the amount of ice lost for multiple samples of forcing on each point of the PP04 limit cycle, impedance can be calculated as the proportion of trajectories which are categorized as partial melts. Another method of measuring impedance could average the amount of ice lost over every sample, as shown in Figure 14b.

This paper presents results for one forcing sample only. With more samples, a distribution of ice loss can be found for each point. From that population, a cutoff can be determined to categorize a run as a full melt or a partial melt. Using this threshold, impedance can be calculated for the PP04 model.

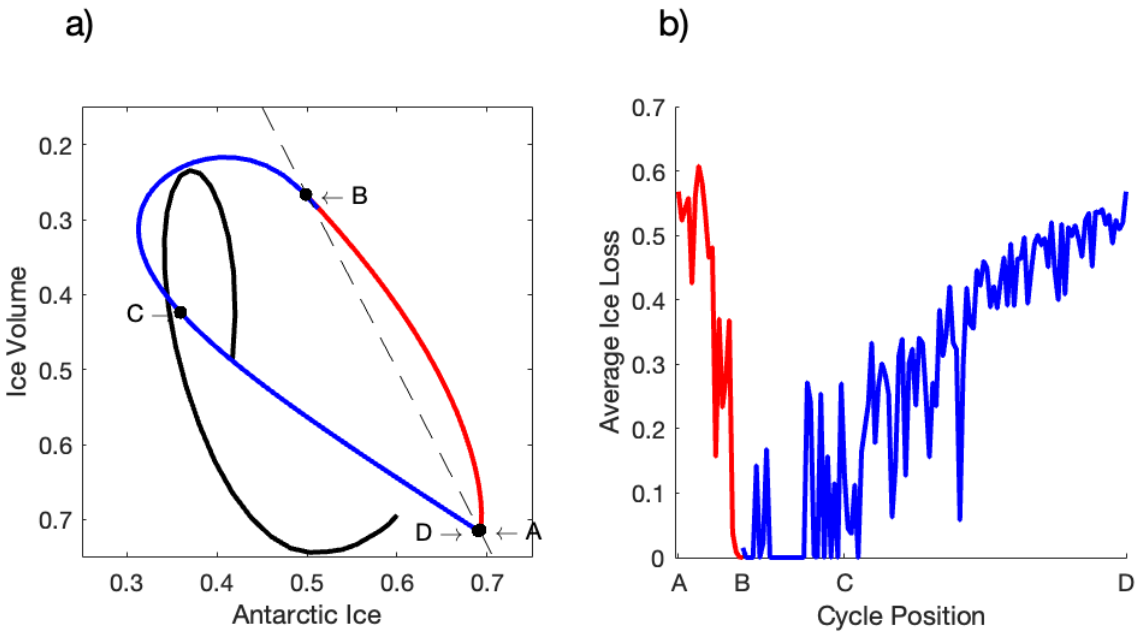

Figure 14: **(a)** One model run using a forcing sample. **(b)** The average ice loss at each point on the PP04 limit cycle, with one sample per point.

4.2.3 Model Synergy

The unforced PP04 model has a periodic limit cycle that represents monotonic warming and cooling within the climate system. Thus, the presence of a partial melt within the system requires the forced trajectory to be working against the natural state of the model. In order to capture this idea with an impedance measure, the dot product of the tangent vector to the forced trajectory and the tangent vector for a free (unforced) trajectory at that point in state space is calculated. When the dot product is large, the model response to the forcing is in synergy with the internal dynamics of the system and a full melt occurs, while a result near zero signifies a partial melt.

To show this behavior in the PP04 model, multiple samples can be taken from the previously constructed population of high insolation events, and the model is run with each sample, using each point on the limit cycle as an initial condition, shown in Figure 15a. The dot product for each trajectory can be calculated temporally, as shown in Figure 15b. Then, the impedance measure looks at the sum of the line integrals for each trajectory's dot product measure. Partial melts result in large dot product measures, and thus larger line integrals, so points with higher impedance will have greater sums.

This paper presents results for five forcing samples applied to one point on the PP04 limit cycle. With more samples, the overall synergy of the PP04 model with possible forcing curves can be determined, to measure impedance.

5 Discussions & Conclusions

This paper explored the data trends of Earth's climate system, which suggested that a slow evolution within the system created an internal impedance to the occurrence of full melts. Obliquity cycles failed to trigger a full melt and instead resulted in partial melts, before the ice rebuilt.

In an effort to create a tool for model validation, this paper sought to quantify the impedance within a model, as a strong model will exhibit impedance in a similar fashion to the global climate system. There were three proposed geometric measures: (1) distance to the trigger line, (2) point perturbation, and (3) gradient perturbation. These measures quantify the impedance inherent to

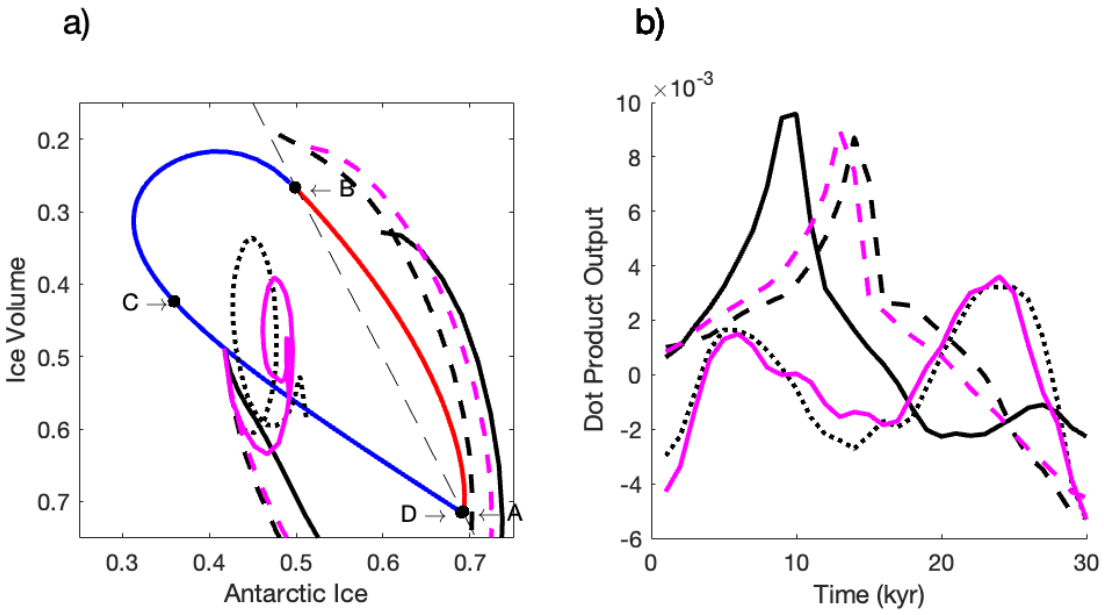

Figure 15: **(a)** Five model runs using forcing samples. **(b)** The dot product output for each of the five runs.

the unforced system of the model, which would arise with the introduction of any arbitrary forcing term.

In order to measure impedance resulting from targeted, more realistic forcing, two measures were proposed: (1) net ice loss and (2) model synergy. Each measure requires a sample of forcing terms pulled from a population of high insolation events, spanning 30 kyr each. Future work remains to test these measures on larger sample sizes, to determine their outputs and efficacy.

The developed impedance measures offer promising options for an impedance-measuring data validation tools. In order to further test, researchers could apply these measures to more models, both smooth and non-smooth. An open question remains as to what an appropriate substitute would be for a trigger line if one does not exist within a model.

References

Alexandrov, D., Bashkirtseva, I., Crucifix, M., & Ryashko, L. Nonlinear climate dynamics: From deterministic behavior to stochastic excitability and chaos. *Elsevier Physics Reports*, 902, 2020.

DOI: https://doi.org/10.5194/egusphere-egu2020-11345

Ashkenazy, Y. & Gildor, H. Timing and significance of maximum and minimum equatorial insolation. *Paleoceanography*, 23, PA1206, 2008. DOI: https://doi.org/10.1029/2007pa001436

Berends, C. J., Köhler, P., Lourens, L. J., & van de Wal, R. S. W. On the cause of the Mid-Pleistocene transition. *Reviews of Geophysics*, 59(2), 2021. DOI: https://doi.org/10.1029/2020rg000727

Berger, A. Long-Term Variations of Daily Insolation and Quaternary Climatic Changes. *Journal of the Atmospheric Science*, 35, 2362–2367, 1978. DOI: https://doi.org/10.1175/1520-0469(1978)035¡2362:LTVODI¿2.0.CO;2.

Crucifix, M. Oscillators and relaxation phenomena in Pleistocene climate theory. *Philosophical Transactions of the Royal Society A: Mathematical, Physical & Engineering Sciences*, 370(1962), 1140-1165, 2012. DOI: https://doi.org/10.1098/rsta.2011.0315

De Saedeleer, B., Crucifix, M., & Wieczorek, S. Is the astronomical forcing a reliable and unique pacemaker for climate? A conceptual model study. *Climate Dynamics*, 40(1-2), 273-294, 2012. DOI: https://doi.org/10.1007/s00382-012-1316-1

Feng, F. & Bailer-Jones, C. Obliquity and precession as pacemakers of Pleistocene deglaciations. *Quaternary Science Reviews*, 122, 166-179, 2015. DOI: https://doi.org/10.1016/j.quascirev.2015.05.006

Gildor, H. & Tziperman, E. Sea ice as the glacial cycles' climate switch: Role of seasonal and orbital forcing. *Paleoceanography*, 15(6), 605-615, 2000. DOI: https://doi.org/10.1029/1999pa000461

Hays, J., Imbrie, J., & Shackleton, .N J. Variations in the Earth's Orbit: Pacemaker of the Ice Ages. *Science*, 194, 1121-1132, 1976. DOI: 10.1126/science.194.4270.1121

Huybers, P., Early Pleistocene Glacial Cycles and the Integrated Summer Insolation Forcing. *Science*, 313, 508-511, 2006. DOI: 10.1126/science.1125249

Huybers, P. Glacial variability over the last two million years: An extended depth-derived agemodel, continuous obliquity pacing, and the Pleistocene progression. *Quaternary Science Reviews*, 26(1-2), 37-55, 2007. DOI: https://doi.org/10.1016/j.quascirev.2006.07.013

Imbrie, J., Hays, J. D., Martinson, D. G., McIntyre, A., Mix, A. C., Morley, J. J., Pisias, N. G., & Prell, W. L. & Shackleton, N. J. The orbital theory of Pleistocene climate: Support from a revised chronology of the marine δ^{18}O record. *Research Gate*, 1984.

Laskar, J., Robutel, P., Joutel, F., Gastineau, M., Correia, A. C., & Levrard, B. A long-term numerical solution for the insolation quantities of the earth. *Astronomy & Astrophysics*, 428(1), 261-285, 2004. DOI: https://doi.org/10.1051/0004-6361:20041335

Leloup, G., & Paillard, D. Influence of the choice of insolation forcing on the results of a conceptual glacial cycle model. *Climate of the Past*, 18(3), 547-558, 2022. DOI: https://doi.org/10.5194/cp-18-547-2022

Lisiecki, L. E. Links between eccentricity forcing and the 100,000-year glacial cycle. *Nature Geoscience*, 3(5), 349-352, 2010. DOI: https://doi.org/10.1038/ngeo828

Lisiecki, L. E., & Raymo, M. E. A Pliocene-Pleistocene stack of 57 globally distributed benthic δ^{18}O records. *Paleoceanography*, 20(1), 2005. DOI: https://doi.org/10.1029/2004pa001071

Milankovitch, M. Canon of insolation and the ice-age problem. *Beograd*, Serbia: Narodna Biblioteka Srbije, 1998. (English translation of the original 1941 publication.)

Paillard, D. The timing of Pleistocene glaciations from a simple multiple-state climate model. *Nature*, 391(6665), 378-381, 1998. DOI: https://doi.org/10.1038/34891

Paillard, D., & Parrenin, F. The Antarctic ice sheet and the triggering of deglaciations. *Earth and Planetary Science Letters*, 227(3-4), 263-271, 2004. DOI: https://doi.org/10.1016/j.epsl.2004.08.023

Past Interglacials Working Group of PAGES. Interglacials of the last 800,000 years. *Reviews of Geophysics*, 54(1), 162-219, 2016. DOI: https://doi.org/10.1002/2015rg000482

Raymo, M. E., & Huybers, P. Unlocking the mysteries of the ice ages. *Nature*, 451(7176), 284-285, 2008. DOI: https://doi.org/10.1038/nature06589

Saltzman, B., & Maasch, K. A. A first-order global model of late Cenozoic climatic change. *Transactions of the Royal Society of Edinburgh: Earth Sciences*, 81(4), 315-325, 1990. DOI: https://doi.org/10.1017/s0263593300020824

Saltzman, B., & Maasch, K. A. A first-order global model of late Cenozoic climatic change II. Further analysis based on a simplification of CO2 dynamics. *Climate Dynamics*, 5(4), 201-210, 1991. DOI: https://doi.org/10.1007/bf00210005

Tziperman, E., Raymo, M. E., Huybers, P., & Wunsch, C. Consequences of pacing the Pleistocene 100 kyr ice ages by nonlinear phase locking to Milankovitch forcing. *Paleoceanography*, 21(4), 2006. DOI: https://doi.org/10.1029/2005pa001241

Von der Heydt, A. S., Ashwin, P., Camp, C. D., Crucifix, M., Dijkstra, H. A., Ditlevsen, P., & Lenton, T. M. Quantification and interpretation of the climate variability record. *Global and Planetary Change*, 197, 103399, 2021. DOI: https://doi.org/10.1016/j.gloplacha.2020.103399

Zachos, J., Pagani, M., Sloan, L., Thomas, E., & Billups, K. Trends, rhythms, and aberrations in global climate 65 ma to present. *Science*, 292(5517), 686-693, 2001. DOI: https://doi.org/10.1126/science.1059412